Impact of GFO Satellite on Naval Antisubmarine Warfare

Dr. Peter C. Chu, LT Guillermo Amezaga
Naval Ocean Analysis and Prediction Laboratory
Naval Postgraduate School, Monterey, California 93940
USA

pcchu@nps.edu

CDR Eric L. Gottshall
Office of Naval Research Global, 223 Old Marylebone Road, London NW1 5TH
United Kingdom

egottshall@onrglobal.navy.mil

Mr. David Cwalina
Naval Undersea Warfare Center, Newport, RI 02841
USA

CwalinaDS@Npt.NUWC.Navy.Mil

ABSTRACT

The purpose of this study is to assess the benefit of assimilating satellite altimeter data especially the US Navy's GFO into the Modular Ocean Data Assimilation System (MODAS). To accomplish this, two different MODAS fields are used by the Weapon Acoustic Preset Program (WAPP) to determine suggested presets for a Mk 48 variant torpedo. The MODAS fields differ in that one uses altimeter data assimilated from three satellites while the other uses no altimeter data. The metric used to compare the two sets of outputs is the relative difference in acoustic coverage area generated by WAPP. Output presets are created for five different scenarios, two Anti-Surface Warfare scenarios and three Anti-Submarine Warfare scenarios, in each of three regions: the East China Sea, Sea of Japan, and an area south of Japan that includes the Kuroshio current. Analysis of the output reveals that, in some situations, WAPP output is very sensitive to the inclusion of the altimeter data because of the resulting differences in the subsurface predictions. The change in weapon presets could be so much that the effectiveness of the weapon might be affected.

1.   INTRODUCTION

The outcome of a battlefield engagement is often determined by the advantages and disadvantages held by each adversary. On the modern battlefield, the possessor of the best technology often has the upper hand, but only if that advanced technology is used properly and efficiently. In order to exploit this advantage and optimize the effectiveness of high technology sensor and weapon systems, it is essential to understand the impact on them by the environment (Mancini, 2004).

Understanding the ocean environment is imperative and directly coupled to the successful performance of ASW sensors and subsequent employment of an ASW weapon system. In order to optimize the performance of ASW sensors and weapons systems, it is crucial to gain an understanding of the acoustic wave propagation in the ocean. Having an accurate depiction of the ocean environment is therefore directly related to gaining a better understanding of the acoustic wave propagation.

How acoustic waves propagate from one location to another under water is determined by many factors, some of which are described by the sound speed profile (SSP). If the environmental properties of temperature and salinity are known over the entire depth range, the SSP can be compiled by using them in an empirical formula to calculate the expected sound speed in a vertical column of water.

The satellites use radiometers to measure the thermal radiation emitted by the sea surface (from which sea surface temperature is derived) and radar altimeters to measure sea surface height (SSH). The satellite data assimilation of SSH into MODAS was previously studied by Chu et al. (2004a) and Chu et al. (2006). Chu et al. (2004a) compared the acoustic coverage of the Generalized Digital Environmental Model (GDEM) and MODAS, with SSH data assimilation, and Perry found that MODAS provided more realistic acoustic coverage than GDEM. Mancini compared the acoustic coverage of MODAS, without SSH data assimilation, and MODAS, with SSH data assimilation. Mancini found that MODAS, with SSH assimilation, provided more realistic acoustic coverage than MODAS, without SSH data assimilation. However, value-added of the Navy's satellite (GFO) on the Naval ASW has not been studied.

MODAS, with SSH data assimilation, gives a better depiction of the ocean environment. Altimeters that have different exact overhead repeat period will have different temporal and spatial resolutions. An altimeter's capability to resolve mesoscale features in the ocean is directly relate to the altimeters exact overhead repeat period. MODAS fields derived from an altimeter with an exact overhead repeat pattern designed to detect mesocale features should be different from MODAS fields derived from an altimeter that is not designed to detect mesocale features, especially in regions of high mesoscale variability. Large differences in the MODAS fields are related to different depictions of the undersea environment. The differences in the depiction of undersea environment may then change the outcome of a tactical engagement.

This study tries to answer the following question: What is the impact of the Navy's satellite (GFO) on the Naval ASW? This question is answered through studying the sensitivity of an ASW weapon system of a naval ASW system, specifically the Mk 48 torpedo WAPP, to satellite altimeter orbit. The sensitivity analysis is conducted by examining the relative difference (RD) in the output of WAPP when two different SSP input fields. The only difference is how to establish these SSP fields, one from MODAS using TOPEX/POSEIDON (T/P) altimetry data and the other from MODAS using GFO altimetry data. The parameters in WAPP are held constant; therefore, any differences in the output were attributed to differences in the input.

The two areas below (Figure1) are selected for analysis because of the high mesocale variability (Figure 2) and tactical significance. The northern box is hereby referred to as the East China Sea (ECS) and is bound by $25°\,\text{N}$, $30°\,\text{N}$, $120°\,\text{E}$, and $130°\,\text{E}$. The southern box is hereby referred to as the South China Sea (SCS) and is bound by $19°\,\text{N}$, $23°\,\text{N}$, $118°\,\text{E}$, and $123°\,\text{E}$. Data analysis was conducted in the ECS and SCS during the winter and summer of 2001. Six days (5, 10, 15, 20 25 and 30) and two months (JAN 2001 and JUL 2001) were selected for analysis in each box. A total of 24 cases (2 areas of interest, 2 months, and 6 days in each month) were analyzed.
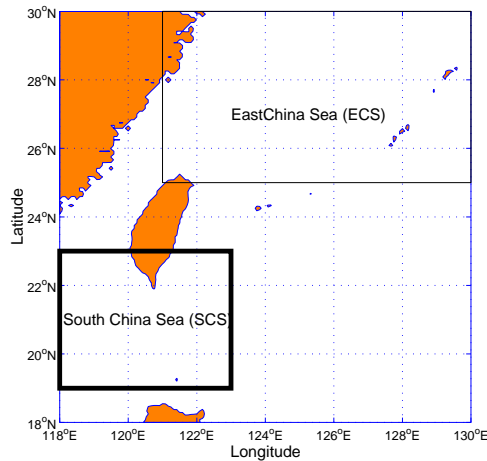
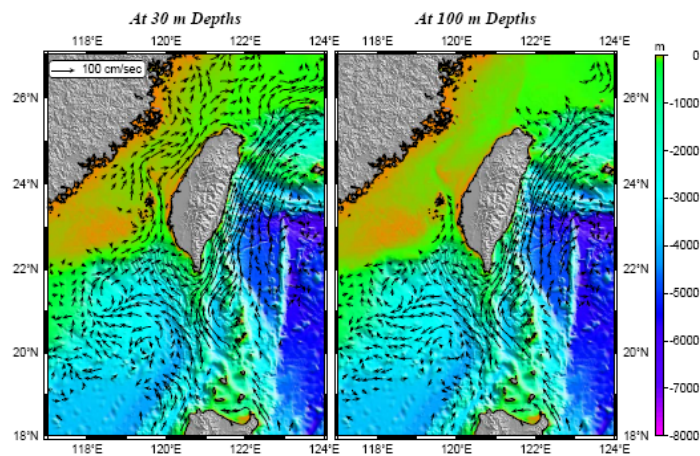**Figure 1. Areas of interest for the analysis.**

Figure 2. Complex subsurface current structure at (a) 30 m, and (b) 100 m deep (after Laing et. al., 2002).

2.   SATELLITE ORBIT ANALYSIS

GFO and TPX satellites have different exact overhead repeat patterns; therefore, GFO and TPX have different temporal and spatial resolutions. Orbit analysis was conducted in the ECS and SCS during the winter and summer of 2001 for both GFO and TPX satellites because of the high mesocale variability and the availability of hydrographic data in the ECS and SCS.

A basic assumption of this study is that GFO is better at detecting mesocale features than TPX. Additionally, it is assumed that greatest difference in the MODAS fields generated by GFO and TPX will be in areas with the high mesoscale variability. Jiang et. al. (1996) showed that spatially dense samples are preferred to temporal frequency samples in resolving mesoscale features in their simulated altimetry experiment for GEOSAT and TPX (Figure 3).
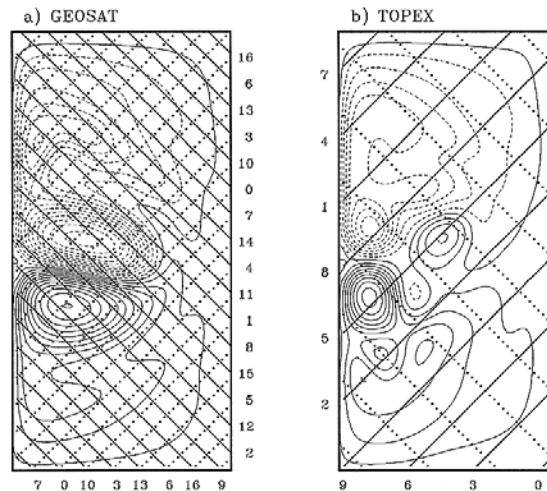
Figure 3. GEOSAT in the left panel provides better resolution of mesoscale features like Western Boundary Currents and eddies than TPX in the right panel (After Jiang et. al., 1996).

2.1 GFO and TX Orbitology

The US Navy launched the GFO satellite in February 1998 from Vandenberg Air Force Base. GFO has an exact overhead repeat (+/- 1 kilometer) of 17 days with an orbit of 800 km, 108 degree inclination, 0.001 eccentricity, and 100-minute period. The US Navy launched GFO to resolve mesoscale features. GFO is capable of tracking the movement of El Nino and La Nina events across the Pacific and resolving Eddies and Western boundary currents.

NASA launched the TOPEX/Poseidon (TPX) satellite on August 10, 1992 for a three-year mission from Kourou, French Guiana. TPX has an exact overhead repeat (+/- 1 kilometer) of 10 days with an orbit of 1336 km, circular, and 66-degree inclination. TPX was initially launched with 3-year mission that was extendable to 6 years. TPX ended up being in orbit for 12 years. JASON-1 was launched in 2001 to replace TPX. JASON-1 shadowed TPX and seamlessly replaced the TPX satellite altimeter.

GFO provides a better spatial resolution than TPX because GFO has a longer exact overhead repeat than TPX (Figure 4). Conversely, TPX provides a better temporal resolution than GFO because TPX has a shorter exact overhead repeat time than TPX. In fact, TPX completes 3 exact overhead repeat cycles during Julian dates 001-030 of 2001, and GFO completes approximately 1.76 exact overhead repeat cycles during Julian dates 001-030 of 2001.

2.2 Orbitology analysis in the ECS and SCS IN January 2001

Figure 5 depicts the orbit tracks for GFO and TPX coverage for ECS and SCS during Julian dates 001-030 in 2001. GFO clearly provides better spatial resolution than TPX because GFO has a spatially dense coverage than TPX for the same time period.
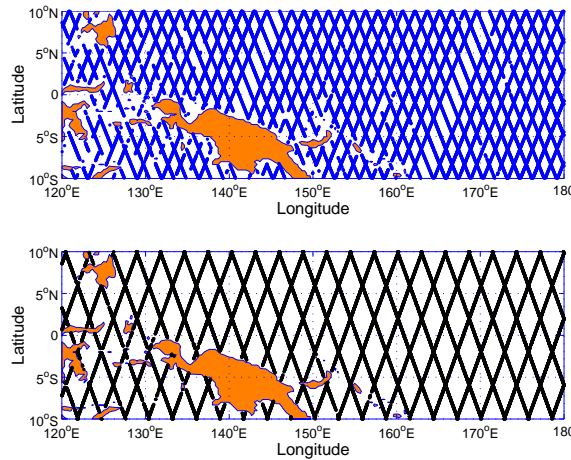
Figure 4. Equator Crossings of GFO (upper panel) and TPX (lower panel) for Julian dates 001-030 in 2001. GFO has better spatial resolution, and TPX has better temporal resolution.
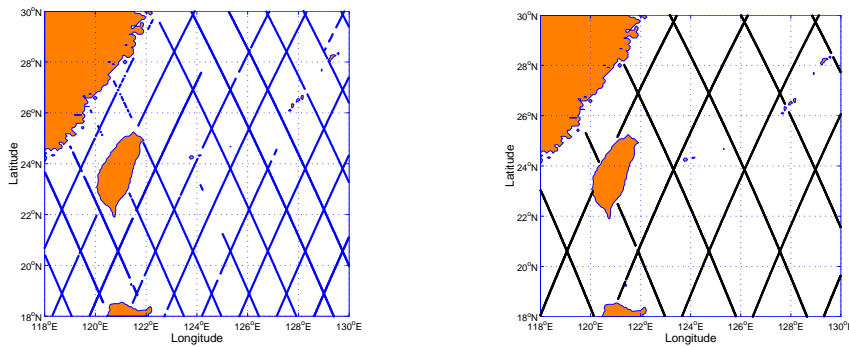

Figure 5. GFO (left) and TPX (right) orbital coverage of the ECS and SCS for Julian dates 001-030 in 2001.

3. MODAS

MODAS is the US Navy's premier dynamic climatology tool. MODAS operates in both a static and dynamic mode. In static mode, MODAS generates a bi-monthly, gridded climatology of temperature and salinity (Fox et al., 2002), which is similar to NOAA's Levitus climatology and the US Navy's Generalized Digital Environmental Model (GDEM). In the dynamic mode, MODAS provides the capability of modifying the historical climatology with remotely sensed SSH and SST, conductivity-temperature-depth (CTD), expendable bathythermograph (XBT), and air dropped expendable bathythermograph (AXBT) temperature and salinity profiles. MODAS can assimilate real-time observations and produce an "adjusted" climatology that more closely represents the actual ocean conditions. The dynamic climatology then provides the end user with nowcast depiction of the ocean's environment (Fox et al., 2002; Chu et al., 2004b).

MODAS resolution ranges from ½ degree to 1/8 degree in gridded output. Since MODAS is comprised of temperature and salinity profiles in the above resolutions, the Sound Speed Profile for each temperature and

salinity pair for each grid point can be calculated empirically, so MODAS provides a three dimensional output of temperature, salinity, and SSP (Fox et al., 2002).

Dynamic MODAS assimilates *in situ* measurements of the temperature and salinity by method known as Optimum Interpolation techniques (Fox et al 2002). OI is a technique used for combining a first guess field and measured data by using a model of how nearby data are correlated. The first guess fields used by MODAS for the OI calculations are the previous day's field for SST and a large-scale weighted average of 35 days of altimetry for SSH. The static climatology is used for the SST first guess. Therefore, synthetic temperature profiles are generated by projecting these fields downward in the water column. The synthetic temperature profiles are projected to a depth of 1500 m utilizing an empirical relationships of the historical data which relates both SST and SSH to the subsurface temperature (Fox et. al., 2002).

Similarly, OI is utilized in the salinity analysis, in situ salinity measurements can then be combined using OI to produce the final salinity analysis (Fox et. al., 2002). The MODAS methodology is outlined in Figure16. The final temperature and salinity analysis are what MODAS uses to produce the other derived fields, such as sound speed.
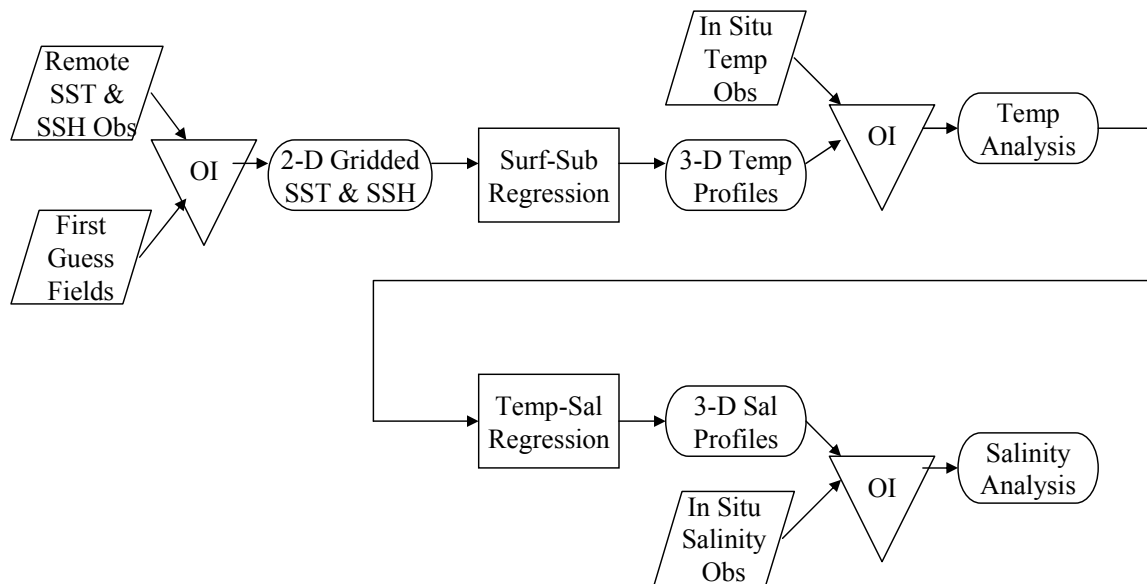

Figure 6. MODAS process flow (after Chu et al., 2006).

4. WEAPON ACOUSTIC PRESET PROGRAM (WAPP) FOR ASW

4.1. Background

Weapon's Acoustic Preset Program provides the US Submarine Fleet with an on-board automated tool for generating the MK 48 and MK 48 ADCAP acoustic presets and visualizing the acoustic coverage for a given torpedo scenario. WAPP is based on Graphic User Interface (GUI) that allows the user to enter environmental, tactical, target, and weapon data. Once the user identifies the above preset for the weapon, WAPP generates a ranked list-set of search depth, search angle, pitch angle, laminar distance, ray trace, and

an acoustic coverage map. The output from the WAPP enables the war-fighter to assess the tactical environment, acoustic environment, weapon presets, and current Target Motion Analysis (TMA).

The MK 48 and MK 48 ADCAP torpedoes utilize High-frequency sonar for search, detection, and homing on a given target. Accurate oceanographic environmental data is needed to correctly predict the acoustic coverage of the MK48 and MK 48 ADCAP torpedoes. The Applied Physics Laboratory and University Washington Technical Report 9407 (APL-UW TR 9407) High-Frequency Ocean Environmental Acoustic Models Handbook was used in programming the WAPP. APL-UW TR 9407 is the bible of High-Frequency modeling. High-Frequency SONAR models must incorporated volumetric sound scattering, sea state, shipping noise, biological ambient noise, and bottom loss to accurately predict acoustic propagation. The affect on acoustic propagation of above oceanographic parameters varies with frequency, so WAPP neglects the Low-Frequency and Medium-Frequency propagation effects and solely predicts the High-Frequency acoustic coverage for the MK 48 and MK 48 ADCAP torpedoes.

4.2. WAPP Ocean Environment Input

Ocean environment data is ingested by the WAPP from various operational oceanographic data sources, oceanographic models, and direct operator inputs. Base on the Date-Time-Group (DTG) and position of the submarine, WAPP extracts the projected environment from the various data sources. Table 1 provides a summary of the data sources used by WAPP. Figure 7 shows the graphic user interface (GUI) of the Environmental Data Entry Module (EDE), which is used by the operator to enter environmental parameters. The EDE is the interface for entry and examination of the Sound Speed Profile (SSP) and entry of Sea State and Bottom Type.

Table 1. WAPP Environment Data Sources.

| WAPP Environment Data Sources	
Data Source	Parameter
DBDB-V v4.2 (Level 2)	(Digital Bathymetric Data Base-Variable) Bottom Depth
GDEM-V v3.0	(Generalized Digital Environment Model) Sound Speed Profile
HIE (SN v5.3)	(Historical Ice Edge) Open Water/MIZ/Ice Cover (Under Ice warfare)
SMGC v2.0	(Surface Marine Gridded Climatology) Historic Wind Speed (Sea State)
BST v1.0	Bottom Sediment Type
VSS v6.3	Volume Scattering Strength Profile
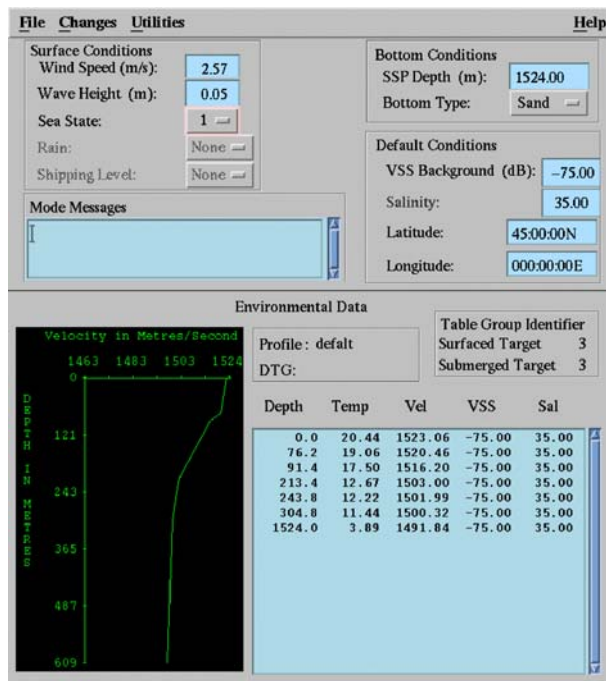
Figure 7. GUI of the Environmental Data Entry Module (EDE).

4.3. WAPP EDE Surface Conditions

The Sea Surface condition is input directly by the operator into the EDE (Figure 8), or the wind speed and wave height is calculated using the World Metrological Organization convention (Table 2). The sea surface condition impacts the WAPP predictions because the acoustic energy suffers forward reflection loss after interacting with the surface (NUWC 2005). Additionally, the active SONAR pulse are reflected by the surface bubbles that increase with sea state; consequently reverberation increases with sea state and target detection decrease with sea state.

Table 2. WMO Convention (Sea State/Wind Speed/ Wave Height)

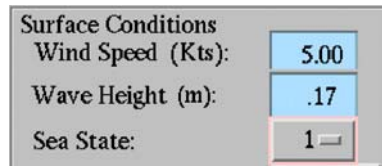| WMO Sea State	Wind Speed (kts)	Significant Wave Height (m)
0	1.5	0
1	5	0.17
2	8.5	0.46
3	13.5	0.91
4	19	1.8
5	24.5	3.2
6	37.5	5.0
7	51.5	7.6
8	59.5	11.4
9	>64	>13.7

Figure 8. WAPP EDE Sea Surface input.

4.4. WAPP EDE Sea Bottom Conditions

The sea bottom entry (Figure 9) consists of the SSP depth and Bottom type. The bottom depth is directly extracted from the SSP. The SSP in use determines the depth. The bottom type button provides the operator the selection of the clay, mud, sand, gravel, and rock. The bottom is characterized by the upper 10 cm for High-Frequency sonar. The Bottom Sediment Type (BST) is undergoing Oceanographic and Atmospheric Mass Library (OAML) certification. Once the BST database is OAML certified, the bottom type will automatically updated in WAPP. Clay and mud bottom have the highest sound attenuation, and the rock bottom has the highest reflection.
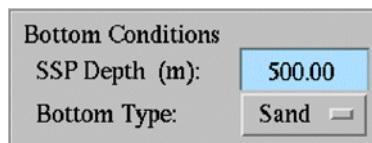

Figure 9. WAPP EDE Sea Bottom Condition.

4.5. WAPP EDE Water Column and Sound Speed Profile Display

WAPP generates a water column characteristics table (Figure10) in the EDE with depth (ft or meters), temperature (degrees Celsius and Fahrenheit), volume scattering strength (dB), and salinity (ppt). WAPP uses an empirical formula in calculating the SSP given two of the three parameters (Temperature, Salinity, or SSP).

| Depth	Temp	Vel	VSS	Sal
.0	68.80	4996.90	-75.00	35.00
213.0	68.80	5000.40	-75.00	35.00
250.0	66.30	4988.40	-75.00	35.00
300.0	63.50	4974.40	-75.00	35.00
500.0	58.50	4949.80	-75.00	35.00
700.0	54.80	4931.10	-75.00	35.00
800.0	54.00	4927.80	-75.00	35.00
1000.0	52.60	4922.30	-75.00	35.00
1500.0	48.30	4902.50	-75.00	35.00

Figure 10. WAPP EDE Water Column input.

5. WAPP ACOUSTIC COVERAGE PREDICTION

The Acoustics Presets Module (Figure 11) is the GUI that allows the operator to set MK 48 tactical presets. The operators identifies tactics, target type (Surface or Submarine), Search Depth, Pitch Angle, search ceiling

and floor, Doppler mode, ping interval, and search mode. Additionally, the operator can refine the Depth Zone of Interest (DZ), acoustic target strength (NTS), acoustic radiated noise of the target (NZE), and the anticipated target Doppler (Dead in Water, Low, High). Base on the variant of the MK 48 selected the by the operator and other ballistic parameters, WAPP displays the ranked list-set calculated with the given environmental inputs, acoustic presets, target type, and ballistic parameters.

WAPP generates a graphical display (Figure 12) of the acoustic coverage base on the inputs in the EDE and Acoustic Preset Module. The acoustic coverage map graphically displays the ray trace, search ceiling and floor, laminar distance, and signal excess.
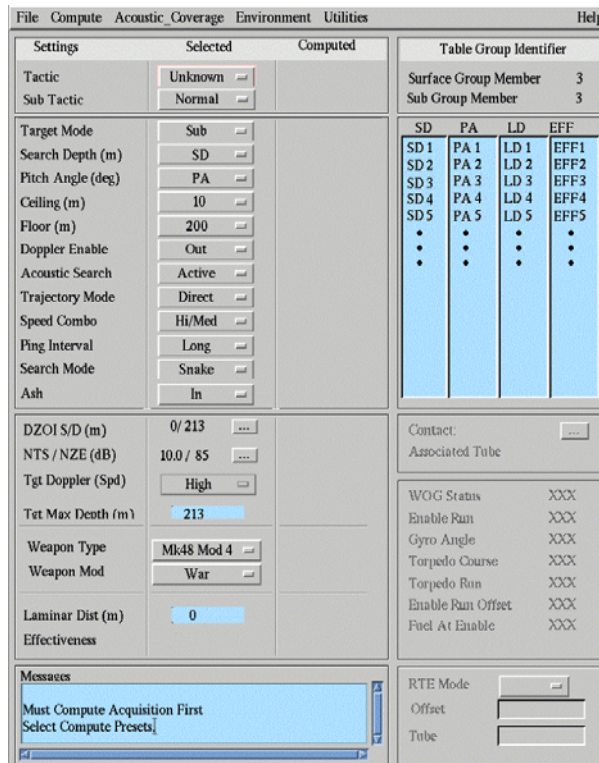
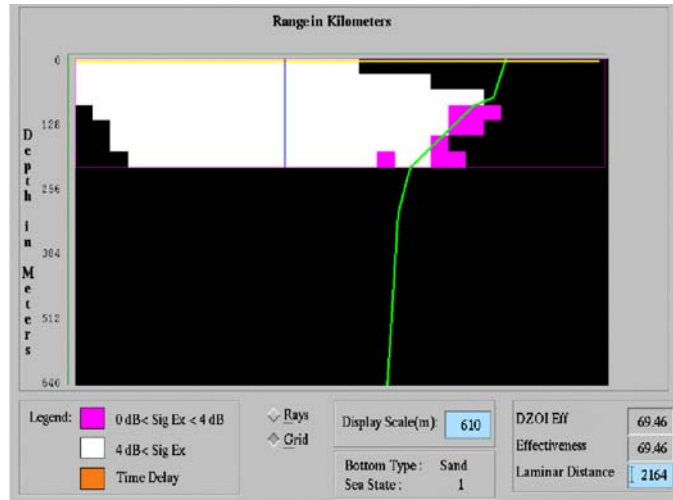**Figure 11. Acoustic Presets Module**

Figure 12. WAPP Acoustic Coverage Map.

The WAPP preset process begins once all input parameters have been selected in the above described GUIs. The process is outlined in Figure 13 (NUWC, 2005, Mancini, 2004). First, valid search depth (SD) and search angle (SA) combinations are computed by utilizing a search angle selection algorithm to identify the optimal pitch angle for each search depth. Second, in series of time steps, the program traces a fan of rays that define the torpedo beam pattern for each resulting SD/SA combination (NUWC, 2005). The signal excess computation is mapped and gridded to the search region at each time step The signal excess map is used to depicts the area coverage (AC) of the search region with signal excess greater than 0 dB (Figure14, white blocks) and 4 db (Figure12, magenta blocks). The laminar distance (Figure12, blue line), signal excess 'center of mass', is also depicted in the signal excess map. Third, WAPP then ranks the SD/SA combinations based on tactical guidance for the weapon and given tactical scenario. Finally, WAPP generates a recommendation based on the ranked list which preset combination is best for the given scenario.
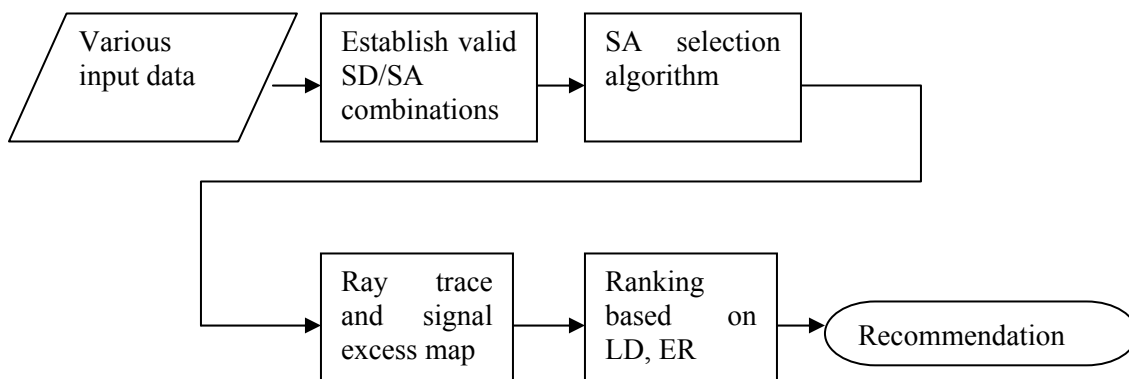

Figure13. WAPP preset process (Chu et al., 2006).

6.   SENSITIVITY OF WAPP TO SATELLITE ORBIT

Figure 14 outlines the flow chart for the WAPP sensitivity analysis for MODAS-GFO and MODAS-TPX datasets. MODAS fields initialized independently with GFO altimetry and TPX sea surface height (SSH) data were compared. The only difference between the MODAS field was the altimetry data. Once again, it is assumed that MODAS fields initialized by GFO (MODAS-GFO) will be more accurate than MODAS fields initialized by TPX (MODAS-TPX). The MODAS-GFO and MODAS-TPX fields were ingested into WAPP to examine the sensitivity of the USW weapon system. The MODAS-GFO fields were used as the benchmark to determine the error statistics for MODAS-TPX. The chief aim of this study is to identify the WAPP sensitivity to altimeter orbit. If there is a large relative difference between MODAS-GFO and MODAS-TPX fields in WAPP, WAPP is sensitive to altimeter orbit.
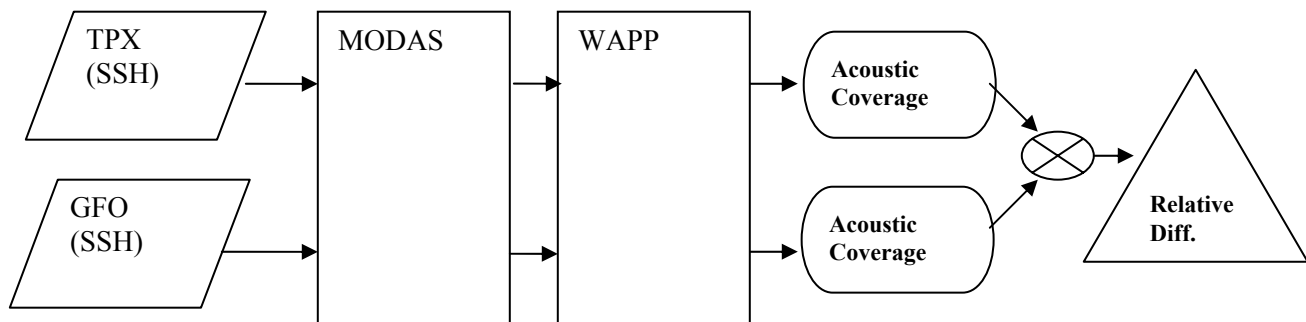

Figure 14. Flow chart of the sensitivity study of WAPP to TPX and GFO Sea Surface Height (SSH).

6.1. MODAS Input Difference

MODAS-GFO and MODAS-TPX data are represented by ψ (temperature, salinity, sound speed (SS)). The difference in ψ between MODAS-TPX and MODAS-GFO data is given by

$$\Delta_m \psi(x_{i,}y_j,z,t) = \psi_{mt}(x_{i,}y_j,z,t) - \psi_{mg}(x_{i,}y_j,z,t) \tag{1}$$

The bias, mean-square–error (MSE), and root-mean-square-error (RMSE) for MODAS,

$$BIAS(mt,mg) = \frac{1}{N}\sum_i\sum_j \Delta_m\psi(x_{i,}y_j,z,t) \tag{2}$$

$$MSE(mt,mg) = \frac{1}{N}\sum_i\sum_j [\Delta_m\psi(x_{i,}y_j,z,t)]^2 \tag{3}$$

$$RMSE(mt,mg) = \sqrt{MSE(mt,mg)} \tag{4}$$

where N is the total number of horizontal points (Chu et al., 2004).

A total of 24 cases were analyzed. A case is comprised of an AOI (ECS or SCS), month (JAN or JUL), and day (5, 10, 15, 20, 25, or 30). Each was individually analyzed.   The case for January 05, 2001 is a

representative case of entire data set. The results of the remainder of the cases can be found in the appropriate appendix. The results are also summarized in table format in the conclusion section.

First, a statistical analysis was conducted on the on the MODAS-TPX and MODAS-GFO fields (SS, temperature, and salinity) before the respective MODAS fields were input into WAPP. The scatter plot (Figure 15) for sound speed (SS) in the SCS on January 05, 2001 demonstrates a clustering around the $SS_{mg} = SS_{mt}$ line. The SS difference between MODAS-TPX and MODAS-GFO demonstrate a Gaussian-type distribution with a mean SS difference of -0.123 m/s and a standard deviation of 2.76 m/s. This result indicates that MODAS-GFO SS is generally faster than MODAS-TPX SS. The RMSD of SS between MODAS-TPX and MODAS-GFO increases from 1m/s at the surface to maximum of 5 m/s at 170 m and then decreases to approximately 0 m/s at 1000 m.

The horizontal difference in sound speed (SS) between MODAS-TPX and MODAS-GFO is depicted in both Figures 16 and 17. Figure 17 depicts the horizontal difference at four depths (75m, 200m, 400m, and 600 m) in the SCS, and the red asterisks indicate the position of the SSPs in Figure 29. Figure 18 is a plot of the SSPs for MODAS-TPX and MODAS-GFO at the indicated position for all depths. For example, in Figures 18(d) and 18(g), MODAS-TPX SSP is faster than MODAS-GFO, and Figure 28 indicates a positive horizontal difference in SSP for the respective positions of Figures 18(d) and 18(g). The general shape of the SSP is the same for both MODAS-TPX and MODAS-GFO; however there is an offset in SSPs for MODAS-TPX and MODAS-GFO.
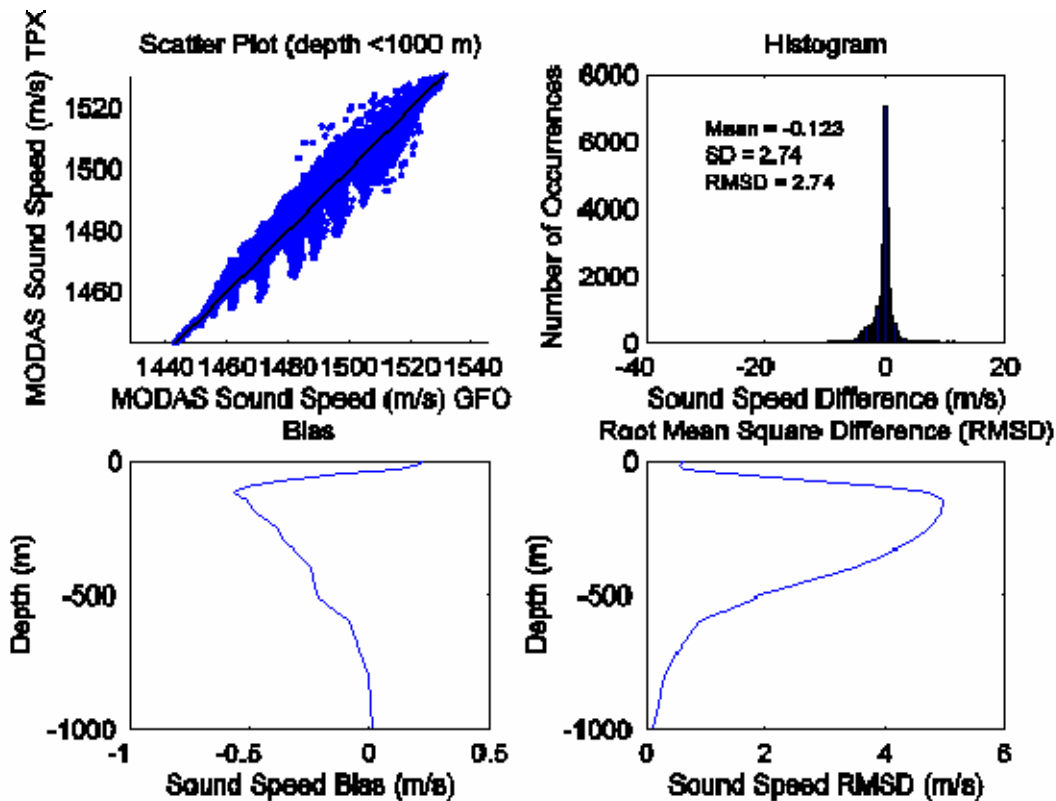

Figure 15. SCS MODAS sound speed statistics for January 05, 2001: (a) scatter plot MODAS-TPX versus MODA-GFO, (b) sound speed difference histogram, (c) sound speed bias, and (d) RMSD of sound speed.

Figure 16. SCS MODAS horizontal difference in SSPs for January 05, 2001. The horizontal difference in SSP (m/s) between MODAS-GFO and MODAS-TPX is depicted at four depths (75m, 200m, 400m, and 600 m). The red asterisk indicates position of SSP in Figure 17.
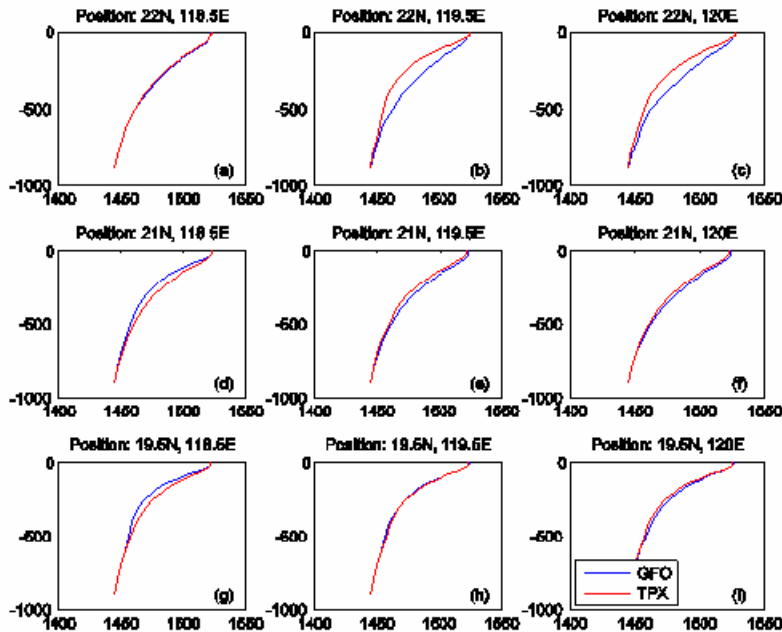
Figure 17. SCS MODAS SSPs for January 05, 2001. The MODAS-TPX SSP is red and MODAS-GFO is blue. The respective SSP is plotted in the position where there was a large positive or negative difference in SSP (red asterisks in Figure 28).

MODAS-TPX and MODAS-GFO SSPs had the largest difference in January 05, 2001 in the SCS, and the difference between MODAS-TPX and MODAS-GFO SSPs continued to decrease through out the month of January 2001. Figures 18 and 19 depict the horizontal difference is SS for January 30, 2001. Both Figures show that horizontal SS difference between MODAS-TPX and MODAS-GFO is decreasing for the SCS. In fact, by inspection of the SSPs for January 05 (Figure 18) and January 30 (Figure 19), the SSPs for MODAS-TPX and MODAS-GFO are converging.

The scatter plot for salinity (Figure 20) demonstrates a clustering around the $S_{mg} = S_{mt}$ line. The errors for temperature demonstrate a Gaussian-type distribution with a mean salinity difference of 0.00114 psu and a standard deviation of 0.0244 psu. This result indicates MODAS-GFO salinity is statically identical to the MODAS-TPX salinity. The RMSD of salinity between MODAS-GFO and MODAS-TPX increases from 0.02 psu at the surface to maximum of 0.06 psu at 300 m and then decreases to 0.05 psu at 1000 m.
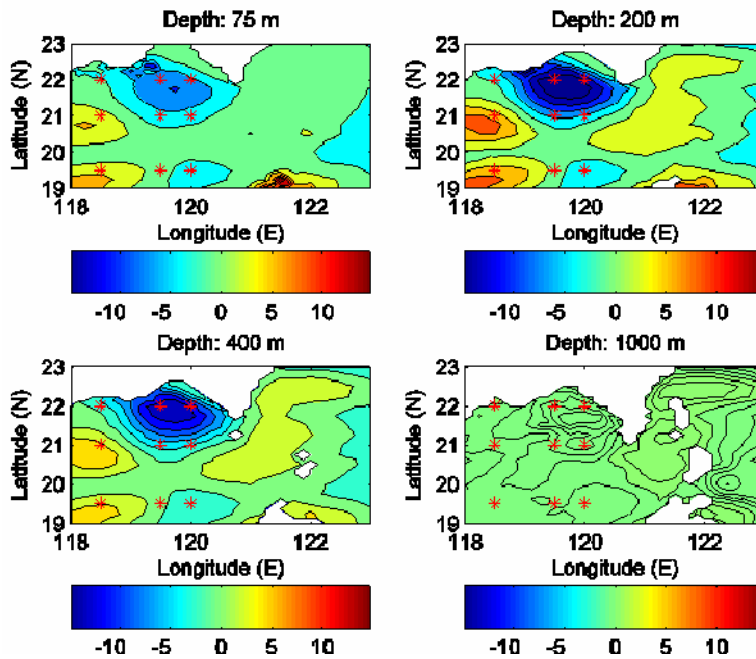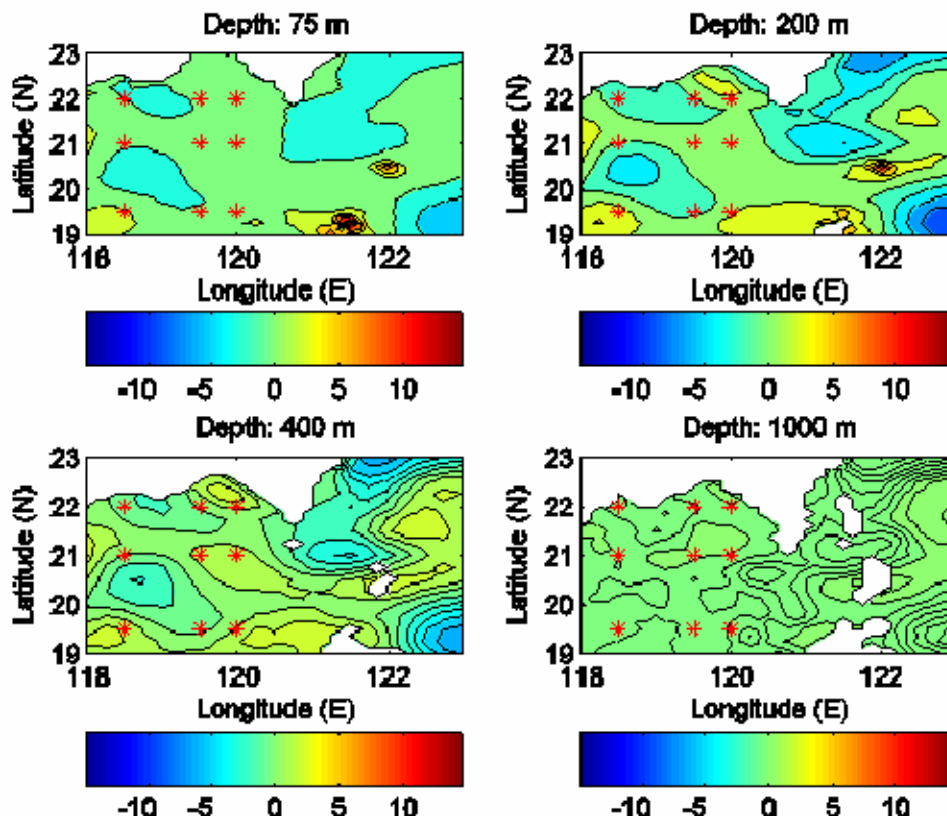
Figure 18. SCS MODAS horizontal difference in SSPs for January 30, 2001. The horizontal difference in SSP (m/s) between MODAS-GFO and MODAS-TPX is depicted at four depths (75m, 200m, 400m, and 600 m). The red asterisk indicates position of SSP in Figure 19.

Figure 19. SCS MODAS SSPs for January 30, 2001. The MODAS-TPX SSP is red and MODAS-GFO is blue. The respective SSP is plotted in the position where there was a large positive or negative difference in SSP (red asterisks in Figure 18).

Figure 20. SCS MODAS salinity statistics for January 05, 2001: (a) scatter plot MODAS-TPX vs MODA-GFO, (b) salinity difference histogram, (c) salinity bias, and (d) salinity speed RMSD.

The scatter plot for temperature (Figure 21) demonstrates a clustering around the $T_{mg} = T_{mt}$ line. The errors for temperature demonstrate a Gaussian-type distribution with a mean temperature difference of $0.0248\,^{\circ}C$ and a standard deviation of $0.628\,^{\circ}C$. This result indicates MODAS-GFO temperature is warmer MODAS-TPX temperature. The RMSD of temperature between MODAS-GFO and MODAS-TPX increases from $0.25\,^{\circ}C$ at the surface to maximum of $1.25\,^{\circ}C$ at 200 m and then decreases to $0.20\,^{\circ}C$ at 1000 m.
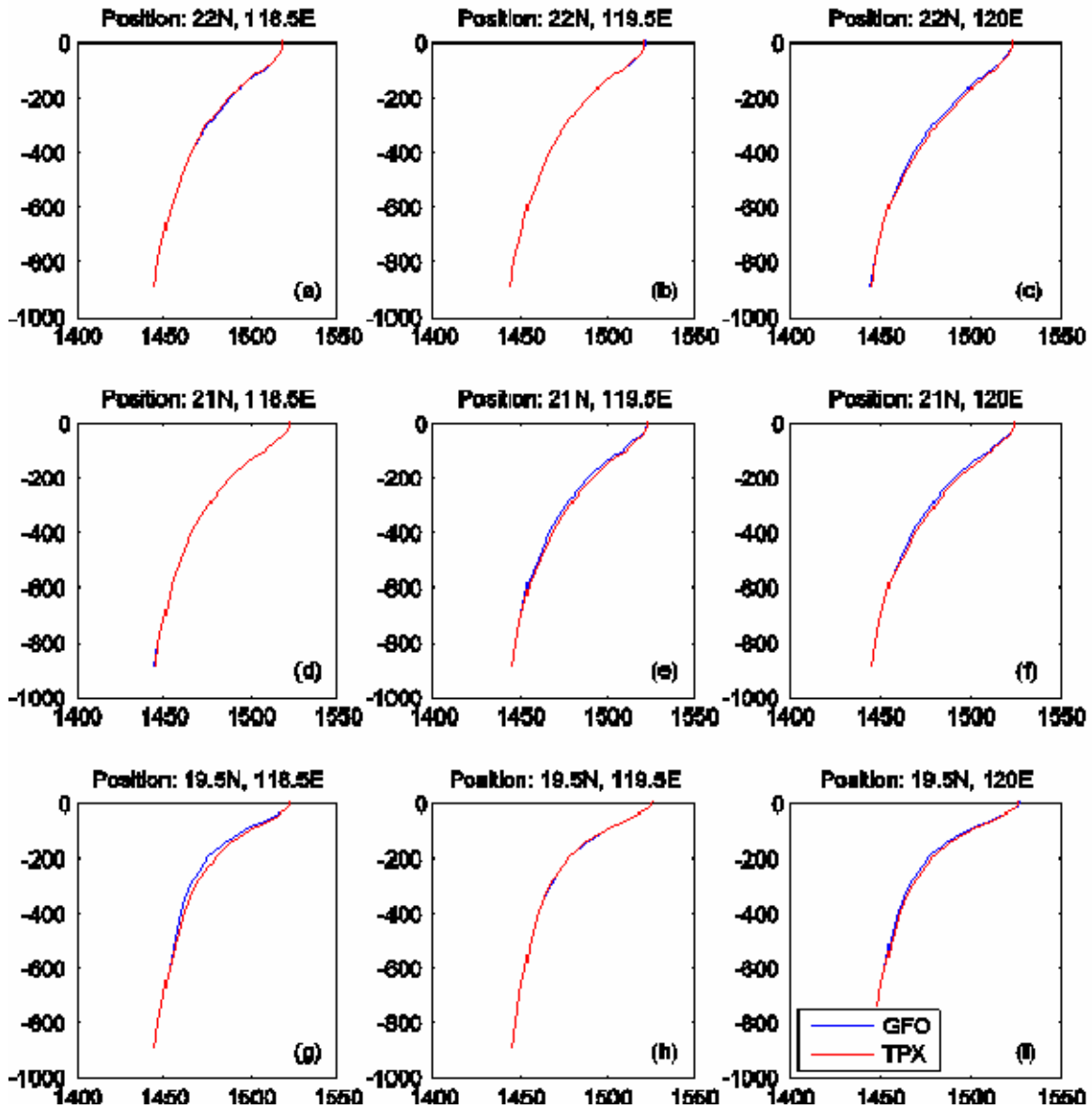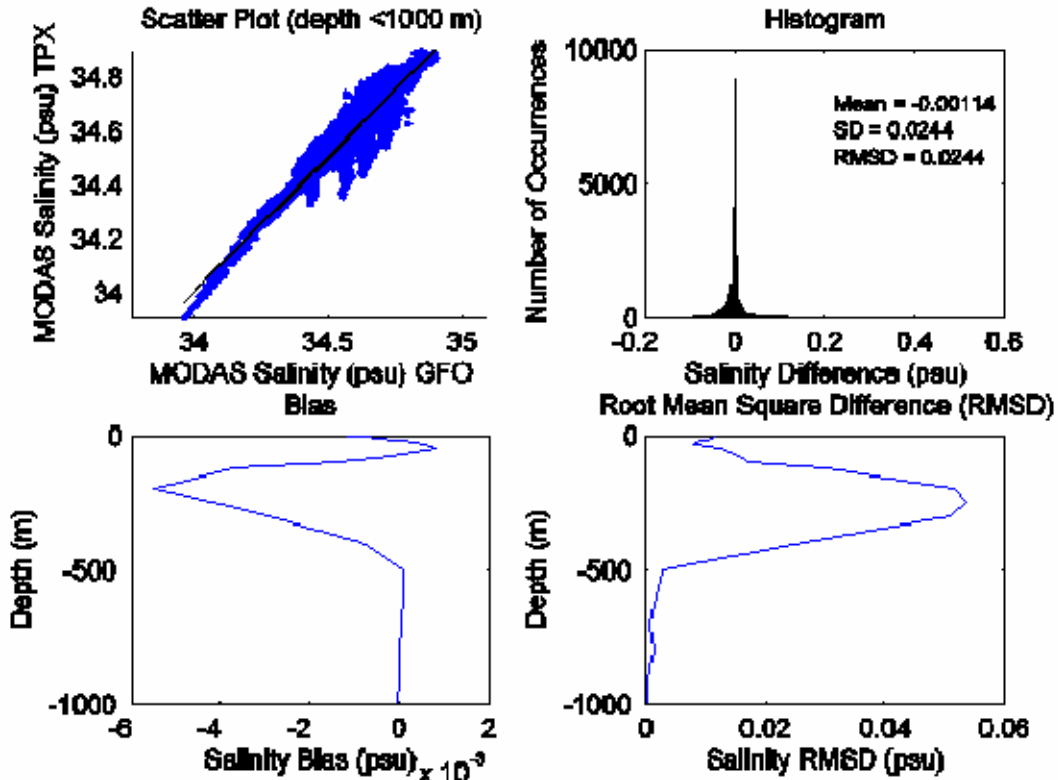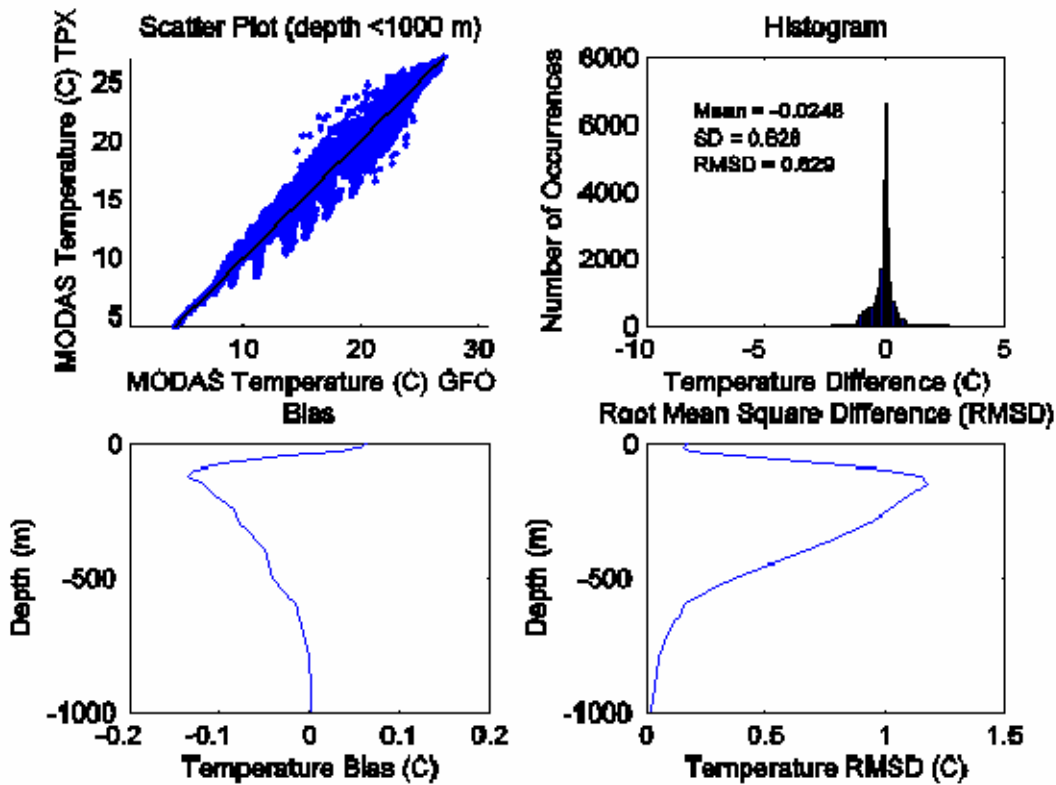
Figure 21. SCS MODAS temperature statistics for January 05, 2001: (a) scatter plot MODAS-TPX vs MODA-GFO, (b) temperature difference histogram, (c) temperature bias, and (d) temperature RMDS.

6.2. WAPP Output Difference

The MODAS-GFO and MODAS-TPX temperature and salinity fields were fed into WAPP. WAPP then calculated the sound speed from the respective temperature and salinity grid point pairs from the respective MODAS fields. The default values in WAPP for volume scattering strength and surface and bottom roughness/reflectivity were used for each tactical scenario. Five different tactical scenarios were selected. The tactical scenarios are selected using the Acoustic Preset GUI (Figure 11). The five tactical scenario selected were high Doppler anti surface warfare (HD ASUW), low Doppler anti surface warfare (LD ASUW), low Doppler shallow anti submarine warfare (LD shallow ASW), high Doppler shallow anti submarine warfare (HD deep ASW), and low Doppler shallow anti submarine warfare (LD deep ASW). Shallow ASW is defined as maximum target depth of 213 meters, and deep ASW is define as maximum target depth of 396 meters (NUWC, 2005). In other words, each of the 24 cases has 5 tactic scenarios (120 tactic scenarios were analyzed), and each tactic scenario was comprised of over 14,000 MODAS-TPX and MODAS-GFO grid point pairs.

Second, WAPP outputs a ranked list-set of different SD/SA combination and acoustic coverage generated for the aforementioned tactical scenario for the respective MODAS-GFO and MODAS-TPX grid point pairs. The same configuration management program used to evaluate POM and MODAS was employed to generate the list set.

Finally, the relative difference was calculated using a statistical package which produced absolute values of the relative differences (RD) in area coverage (AC) for the identical SD/SA combination generated by WAPP,

$$RD = \frac{\left| AC_{mg} - AC_{mt} \right|}{AC_{mg}}. \tag{5}$$

Here, the subscripts *mg* denotes MODAS-GFO and *mt* denotes MODAS-TPX.

WAPP generated SD/SA combinations that were the same and some that were different. The SD/SA combinations that were the same but had a different acoustic coverage were attributed to differences in the ocean's environment (NUWC, 2005). The SD/SA combinations that were different and had different acoustic coverage were attributed to differences in torpedo target motion analysis (TMA) and ballistics. So, any differences in the output were attributed to differences in the input because all other parameters were constant (NUWC, 2005).

Initially, it was assumed that a RD in acoustic coverage of 20% will significantly change the outcome of a tactical engagement. Figure 22 depicts two cases where there is a 20 % difference of acoustic coverage in the torpedo acoustic cone (NUWC, 2005). The two cases depicted in Figure 22 are a screen capture of torpedo engagement simulation in MATLAB conduct by the Naval Undersea Warfare Command (NUWC, Newport). Each dot is a probable contact and is red until the acoustic cone of the torpedo passes over the dot. The dot turns yellow when the torpedo has a detection opportunity. The torpedo then enters into its detection, acquisition, and verification phases. If a dot remains in the acoustic cone long enough to complete the detection, acquisition, and verification phases, the torpedo will likely enter homing, a green dot.

In the first case (Figure 22a), 94.2% of tracks enter the acoustic cone and 46.7% enter homing with an overall coverage score of 47.7 %. In the second case (Figure 34b), when the acoustic coverage was reduce by 20%, 89.6% of tracks enter the acoustic cone and only 16.3% enter homing with an overall coverage score of 33.8%. In other words, a relative difference greater than 20% leads to an engagement that is 1/3 as likely to lead to mission success. So, a relative difference of 20% is large enough to change an engagement. A speculative regression curve that is bound by the by first and second case infers that a RD of between 10 and 15 percent would yield an overall coverage score between 47.7% and 33.8%.

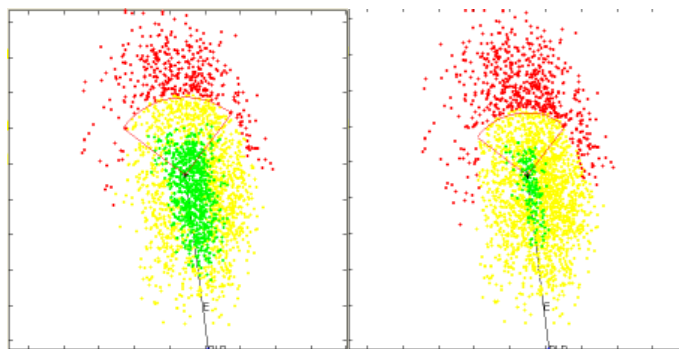**Figure 22. Horizontal acoustic coverage map. The two case depicted a typical acoustic cone for (a) torpedo and (b) acoustic cone reduced by 20%. A red indicates a probable contact. A red dot turns yellow when the torpedo has a detection opportunity. If a dot remains in the acoustic cone long enough to complete the detection, acquisition, and verification phases, the torpedo will likely enter homing, a green dot.**

Data analysis proved that most the cases studied herein had a low probability that the RD is greater than 20%. A histogram of RD displays the number of same SD/SA combinations with area coverage relative differences in specified ranges, or bins, and the probabilities of RD being greater than 0.1 and 0.15

$$\mu_1 = \text{Prob}\,(RD > 0.10), \quad \mu_2 = \text{Prob}\,(RD > 0.15), \tag{6}$$

are then used for the determination of the sensitivity.

6.3.   Different Scenarios

The results for the 24 cases analyzed have the same general trend. Similar to the results from Mancini, 2004, the ASUW scenarios had larger relative differences than the ASW scenarios. Mancini found the probability values (RD) decrease with increasing tactic depth band. In all scenarios, the probability values decreased with increasing tactic band; Figure 23 depicts that all three ASW scenarios have lower probability values than the ASUW scenarios for January 05, 2001.

The histogram of the HD ASW scenario (Figure 24), lowest probability value, on January 05, 2001 had a mean RD of 4.60 with a standard deviation of 2.58, or the mean value of the relative difference between the two acoustic coverages generated by MODAS-TPX and MODAS-GFO in the HD ASW scenario is 4.60%. The histogram HD ASUW (Figure 25), highest probability value, for January 05, 2001 has mean RD of 6.60 with a standard deviation of 4.88.
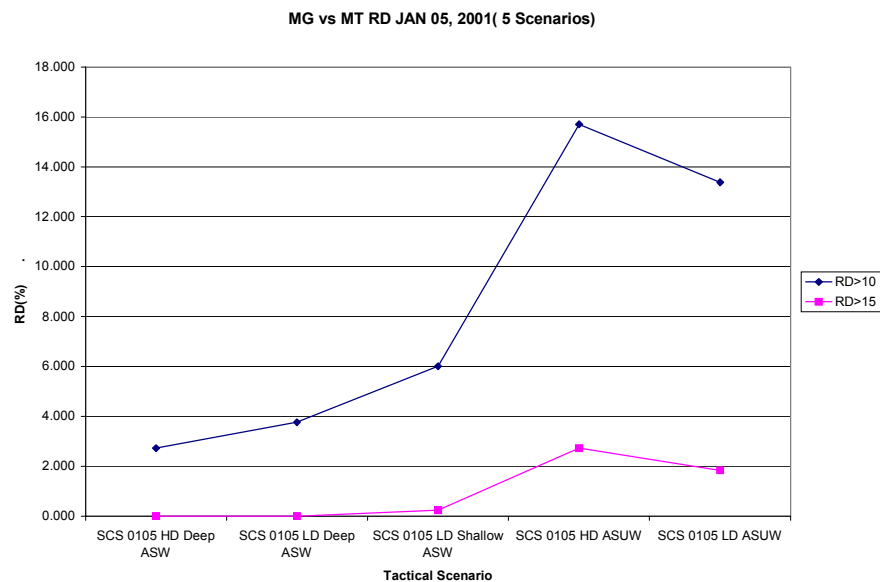

Figure 23.   Probability curve SCS January 05, 2001.
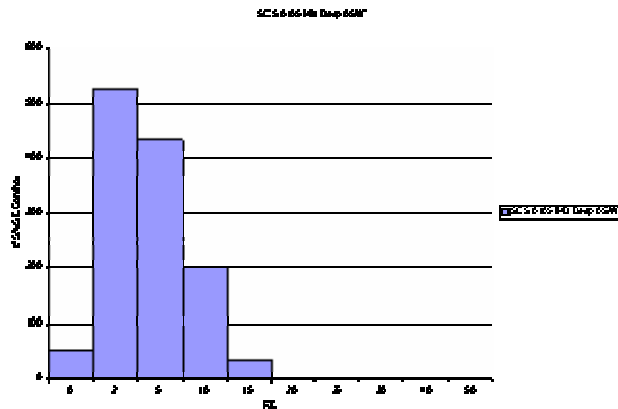
Figure 24. Wapp output for the relative difference between MODAS-TPX and MODAS-GFO for the HD deep ASW scenario. Mean is 4.60, standard deviation is 2.58.
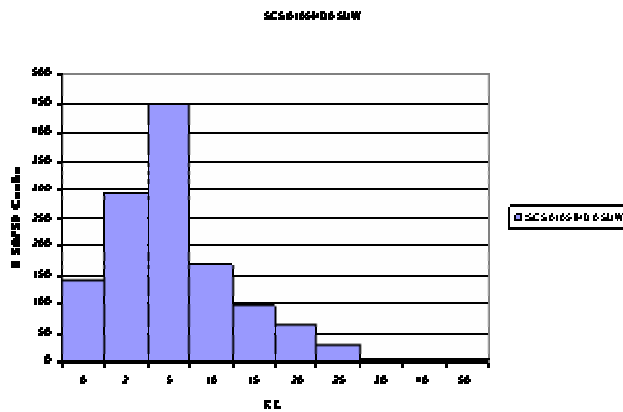
Figure 25. Wapp output for the relative difference between MODAS-TPX and MODAS-GFO for the HD ASUW scenario. Mean is 6.60, standard deviation is 4.88.

The mean RD for all five tactical scenarios for January 2001 in the SCS (Figure 26) and the ECS (Figure 27) are decreasing as function of time. The mean RD for all cases in both the ECS and SCS are less than 6.60 %. Tables 4 and 5 are a summary of the sensitivities of the all the tactic scenarios in January for both the ECS and SCS. In the 60 tactic scenarios in Tables 4 and 5, the mean RD for all tactic scenarios is less than 6.68 (SCS 0110 HD ASUW). Furthermore, the probability that the RD is greater that 15 is less than 4.01% (SCS 0110 HD ASUW) for all 60 tactic scenarios in January, and the probability that the RD is greater that 10 is less than 17.01% for all 60 tactic scenarios in January.
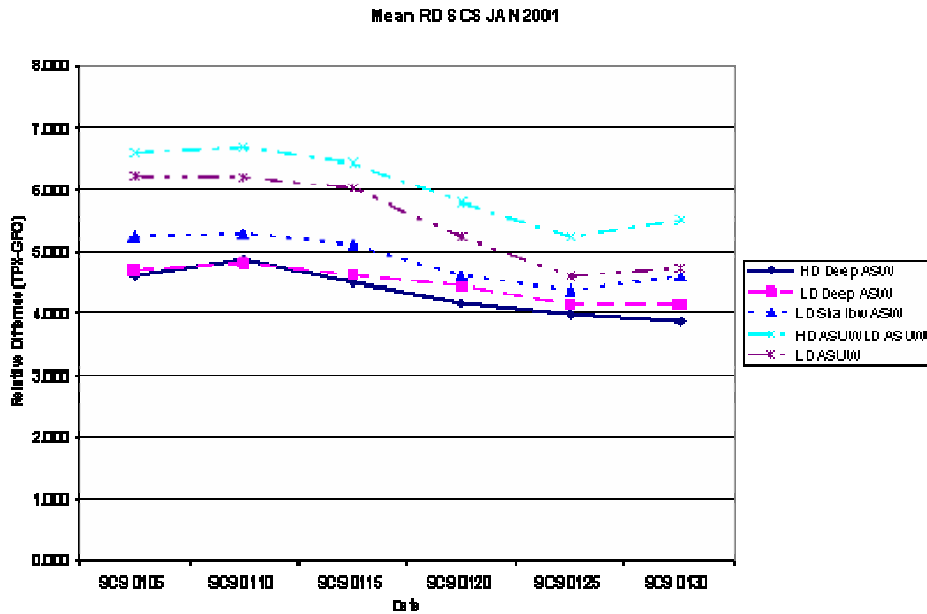
Mean RD SCS JAN 2001

Figure 26. Mean RD in the SCS January 2001.

Mean RD ECS JAN 2001 (5 Scenarios)
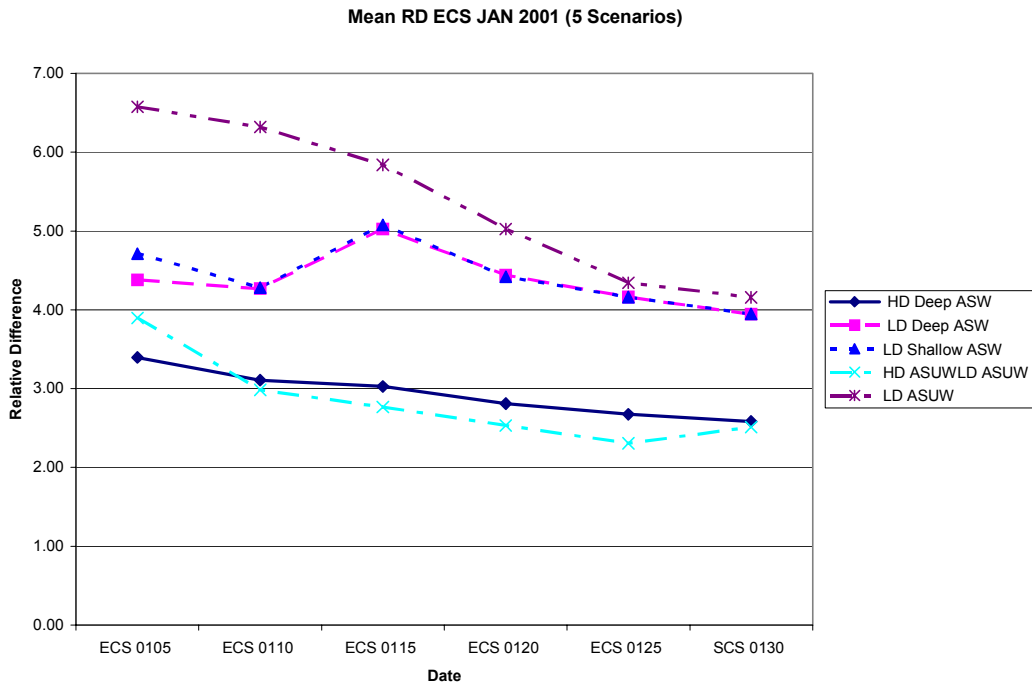
Figure 27. Mean RD in the ECS January 2001.

Table 3. WAPP output differences between GFO and TPX for the SCS January 2001.

	Prob(RD>10)	Prob(RD>15)	Mean RD	SD
SCS 0105 HD Deep ASW	2.72	0.00	4.60	2.59
SCS 0110 HD Deep ASW	3.04	0.08	4.87	2.73
SCS 0115 HD Deep ASW	2.08	0.08	4.50	2.60
SCS 0120 HD Deep ASW	0.56	0.00	4.16	2.25
SCS 0125 HD Deep ASW	0.80	0.00	3.97	2.31
SCS 0130 HD Deep ASW	0.32	0.00	3.86	2.10

	Prob(RD>10)	Prob(RD>15)	Mean RD	SD
SCS 0105 LD Deep ASW	3.77	0.00	4.69	2.75
SCS 0110 LD Deep ASW	3.69	0.08	4.81	2.87
SCS 0115 LD Deep ASW	2.72	0.08	4.61	2.66
SCS 0120 LD Deep ASW	1.28	0.08	4.44	2.46
SCS 0125 LD Deep ASW	1.04	0.08	4.15	2.36
SCS 0130 LD Deep ASW	0.88	0.00	4.14	2.29

	Prob(RD>10)	Prob(RD>15)	Mean RD	SD
SCS 0105 LD Shallow ASW	6.01	0.24	5.23	3.30
SCS 0110 LD Shallow ASW	5.85	0.32	5.28	3.21
SCS 0115 LD Shallow ASW	3.77	0.32	5.11	3.05
SCS 0120 LD Shallow ASW	2.16	0.16	4.60	2.71
SCS 0125 LD Shallow ASW	2.88	0.24	4.37	2.81
SCS 0130 LD Shallow ASW	3.37	0.24	4.59	2.87

	Prob(RD>10)	Prob(RD>15)	Mean RD	SD
SCS 0105 HD ASUW	15.71	2.72	6.60	4.88
SCS 0110 HD ASUW	15.63	**4.01**	**6.68**	5.19
SCS 0115 HD ASUW	13.86	2.32	6.44	4.82
SCS 0120 HD ASUW	10.74	0.80	5.79	4.14
SCS 0125 HD ASUW	6.97	0.40	5.22	3.60
SCS 0130 HD ASUW	7.77	0.48	5.51	3.52

	Prob(RD>10)	Prob(RD>15)	Mean RD	SD
SCS 0105 LD ASUW	13.38	1.84	6.23	4.58
SCS 0110 LD ASUW	13.06	0.96	6.22	4.18
SCS 0115 LD ASUW	11.22	1.20	6.02	4.21
SCS 0120 LD ASUW	7.45	0.80	5.23	3.67
SCS 0125 LD ASUW	5.21	0.72	4.59	3.47
SCS 0130 LD ASUW	4.49	0.80	4.73	3.47

Table 4. WAPP output differences between GFO and TPX for the ECS in January 2001.

	Prob(RD>10)	Prob(RD>15)	Mean RD	SD
ECS 0105 HD Deep ASW	0.94	0.00	3.40	2.75
ECS 0110 HD Deep ASW	0.80	0.00	3.11	2.55
ECS 0115 HD Deep ASW	0.37	0.00	3.03	2.24
ECS 0120 HD Deep ASW	0.09	0.00	2.81	1.99
ECS 0125 HD Deep ASW	0.14	0.00	2.68	2.00
ECS 0130 HD Deep ASW	0.09	0.00	2.59	1.98

	Prob(RD>10)	Prob(RD>15)	Mean RD	SD
ECS 0105 LD Deep ASW	5.29	0.89	4.38	4.45
ECS 0110 LD Deep ASW	5.90	0.89	4.27	4.58
ECS 0115 LD Deep ASW	9.08	2.15	5.03	6.30
ECS 0120 LD Deep ASW	6.18	2.76	4.44	6.22
ECS 0125 LD Deep ASW	5.52	2.29	4.16	6.03
ECS 0130 LD Deep ASW	4.92	2.43	3.94	5.79

	Prob(RD>10)	Prob(RD>15)	Mean RD	SD
ECS 0105 LD Shallow ASW	5.81	0.84	4.71	4.68
ECS 0110 LD Shallow ASW	6.51	0.94	4.28	4.78
ECS 0115 LD Shallow ASW	9.97	2.15	5.08	6.47
ECS 0120 LD Shallow ASW	6.98	2.81	4.42	6.39
ECS 0125 LD Shallow ASW	6.23	2.29	4.16	6.18
ECS 0130 LD Shallow ASW	5.52	2.43	3.95	5.91

	Prob(RD>10)	Prob(RD>15)	Mean RD	SD
ECS 0105 HD ASUW	5.76	1.08	3.90	4.60
ECS 0110 HD ASUW	5.24	0.89	2.99	4.59
ECS 0115 HD ASUW	4.12	0.80	2.76	4.29
ECS 0120 HD ASUW	3.28	0.05	2.53	3.76
ECS 0125 HD ASUW	2.39	0.14	2.31	3.49
ECS 0130 HD ASUW	3.32	0.19	2.51	3.87

	Prob(RD>10)	Prob(RD>15)	Mean RD	SD
ECS 0105 LD ASUW	**17.51**	3.60	6.57	7.72
ECS 0110 LD ASUW	15.03	3.89	6.32	7.84
ECS 0115 LD ASUW	13.90	3.89	5.84	7.18
ECS 0120 LD ASUW	10.96	3.09	5.03	6.64
ECS 0125 LD ASUW	8.47	1.69	4.35	5.79
ECS 0130 LD ASUW	7.82	1.22	4.16	5.46

7. CONCLUSIONS

The chief aim of this study was to determine the sensitivity of an USW system to altimeter orbit. Two area of interest with high mesoscale variability were analyzed. A key assumption of this study is that GFO has better spatial resolution than TPX; therefore, it was assumed that MODAS fields initialized with GFO sea surface heights are more accurate than MODAS fields initialized with TPX sea surface heights. A second assumption is that greatest relative difference in acoustic coverage in WAPP will be in areas of high mesoscale variability.

In conclusion, there is small probability(less than 18 %) that the RD is greater 10 between MODAS-TPX and MODAS-GFO for all scenarios. It appears that the USW weapon system is not overly sensitive to altimeter orbit. That is not to say, that altimeter orbit is not important. The spatially dense altimeter sampling is preferred over temporal frequency sampling to resolve mesoscale features. The resolving of mesoscale features in essential to the warfighter at the strategic level. At strategic level, the warfighter is concerned with placement of assets, where to conduct operations, where the enemy submarine is hiding and so on. The US Navy's USW weapons is technological advance, so it appears that, in the case of different altimeter orbits, the USW weapon system is adequately robust to overcome the difference in between the two altimeters.

ACKNOWLEDGMENTS

REFERENCES

Amezaga, G. R., "Impact of GFO Satellite and Ocean Nowcast/Forecast Systems on Naval Antisubmarine Warfare", MS Thesis, Naval Postgraduate School, March, 2006.

Applied Physics Laboratory University of Washington (APL-UW). *APL-UW High-Frequency Ocean Environmental Acoustic Models Handbook (TR 9407)*. Seattle, Washington: APL-UW, 1994.

Chu, P. C., M. D. Perry, E.L. Gottshall, and D. S. Cwalina. "Satellite data assimilation for improvement of Naval undersea capability." Marine Technological Society Journal, 38 (1), 11-23, 2004a.

Chu, P. C., W. Guihua, C. Fan. "Evaluation of the U. S. Navy's Modular Ocean Data Assimilation System (MODAS) Using South China Sea Monsoon Experiment (SCSMEX) Data." Journal of Oceanography, 2004b.

Chu, P.C., S. Mancini, E.L. Gottshall, D.S. Cwalina, and C.N. Barron. "Sensitivity of satellite altimetry data assimilation on a weapon acoustic preset." IEEE Journal of Oceanic Engineering, in press, 2006.

Fox, D. N., W. J. Teague, C. N. Barron, M. R. Carnes, and C. M. Lee. "The Modular Ocean Data Assimilation System (MODAS*)." *Journal of Atmospheric and Oceanic Technology* 19 (February 2002): 240-252.

Fox, D. N., C. N. Barron, M. R. Carnes, M. Booda, G. Peggion, and J. Gurley. "The Modular Ocean Data Assimilation System." *Oceanography* 15 (No. 1 2002a): 22-28.

Fox, Dan N. MODAS Homepage: http://www7320.nrlssc.navy.mil/modas/ Accessed 25 December, 2005.

Jacobs, G. A., M. R. Carnes, D. N. Fox, H. E. Hurlburt, R. C. Rhodes, W. J. Teague, J. P. Blaha, R. Crout, O. M. Smedstad, Naval Research Laboratory Report NRL/MR/7320-96-7722, Warfighting Contributions of the Geosat Follow-On Altimeter, 1996.

Jacobs, G. A., C. N. Barron, M. R. Carnes, D. N. Fox, H. E. Hurlburt, P. Pistek, R. C. Rhodes, and W. J. Teague, Naval Research Laboratory Report NRL/FR/7320-99-9696, Navy Altimeter Requirements, 1999.

Jiag, S., M. Ghil, "Tracking Nonlinear Solutions with Simulated Altimetric Data in a Shallow-Water Model." *J. Phys. Oceanogr:* Vol. 27, No. 1, pp. 72-95,1996.

Liang, W. -D., T. Y. Tang, Y. J. Yang, M. T. Ko, W.-S. Chuang, "Upper-ocean currents around Taiwan." *Deep-Sea Research II 50 (2003):*1085-1105.

Murphy, A. H., 1988, "Skill score based on the mean square error and their relationships to the correlation coefficient. *Mon Wea. Rev.*, 116, 2416-2424.

Naval Undersea Warfare Center (NUWC). WAPP overview, PowerPoint view graphs, 2005.